CFD Analysis of a Microturbine Combustor using an LES Turbulence Model

Kvale, M.

June 21, 2020

University of Bergen
Geophysical Institute

Western Norway University of Applied Sciences
The Faculty of Engineering and Sciences

Bergen, June 2020

CFD Analysis of a Microturbine Combustor using an LES Turbulence Model

Kvale, M.

University of Bergen (UiB)
The Faculty of Mathematics and Natural Sciences
Geophysical Insitute
Post Box 7803
5020 Bergen, Norway

In cooperation with:
Western Norway University of Applied Sciences (HVL)
The Faculty of Engineering and Sciences
Department of Mechanical and Marine Engineering (IMM)
Post Box 7030
5020 Bergen, Norway

Norwegian Title:	CFD Analyse av Brennkammer i Gassturbin med bruk av en LES Turbulensmodell

Author:	Mikhael Kvale
Student Number:	243862

Program:	Master Programme in Energy, Thermal Machines
Course:	ENERGI
Credits:	30
Date of Submission:	21.06.2020

Supervisor at HVL:	Associate Professor Shokri Amzin
Supervisor at UiB:	Professor Bjørn Johan Arntzen

Number of documents submitted:	1
Working files submitted:	3

Preface

This 30 credit master thesis was written over the course of one semester and submitted as part of the master's programme in Energy with specialization in Thermal Machines. The programme is a cooperation between the Department of Mechanical and Marine Engineering at Western Norway University of Applied Sciences and University of Bergen.

The thesis work was supervised by Associate Professor Shokri Amzin at Western Norway University of Applied Sciences and co-supervised by Professor Bjørn Arntzen at University of Bergen. The topic for the thesis was numerical simulation using computational fluid dynamics (CFD) of a combustor in a microturbine which was designed at the university a few years prior. CFD simulation is a relatively new technology and related literature, especially using modern turbulence models, is fairly limited. During the course of the semester, the corona virus outbreak occured and most businesses and insitutions operated in reduced capacity. This made the project more challenging as most of the work had to be performed from home and there was no possiblity of meetings in person for consulting. Despite the unfortunate circumstances, the process was both interesting and highly educative.

I would like to acknowledge and express my gratitude to the following people for their support during the project:

Associate Professor Shokri Amzin for being solutions-oriented and provide valuable feedback.

Professor Bjørn Arntzen for valuable feedback on chemical reactions, turbulent flow theory and scientific writing.

Professor Boris Balakin for introducing me to CFD simulation using STAR-CCM+ and providing me technical support related to the software.

I also wish to extend my thanks to my fellow student Thomas Samnøy for helping me with LaTeX and keeping spirits high. Finally I wish to express my gratitude to my dear wife Fatima Kvale, for her continous motivational support.

Abstract

This thesis provides a brief overview of the most common methods used for numerical analysis of turbulent flows. The process of setting up a simulation of the reacting process in a microturbine combustor using an LES turbulence model is described. The software tool used in this work is Siemens' STAR-CCM+. A volume mesh is generated for the combustor model and the reaction chemistry is set up using propane as fuel. In addition, a previously performed experimental setup using the same combustor is briefly presented. The objective of the simulation is to provide a temperature and velocity profile for the combustor and to determine the mass fraction of emissions. The results showed the combustion process developing into a stable state over the course of approximately 300ms. The combustor has a uniformly distributed temperature profile, albeit with some high temperature levels in the flametube and outlet, causing some formation of NO_x. In the last part of the thesis, the results from the simulation and experiment are discussed.

List of Abbrevations

AFR	Mass Air/Fuel Ratio
C_3H_8	Propane
CFD	Computation Fluid Dynamics
CO	Carbon Monoxide
CO_2	Carbon Dioxide
CPU	Central Processing Unit
DNS	Direct Numerical Simulation
H_2O	Water
LES	Large Eddy Simulation
Ma	Mach Number
NO_x	Nitrogen Oxides
PDF	Probability Density Function
PM	Particulate Matter
RAM	Random Access Memory
RANS	Reynolds-averaged Navier-Stokes
RPM	Revolutions per Minute
SCR	Selective Catalytic Reduction
SO_2	Sulfur Dioxide
SLF	Steady Laminar Flamelet
UHC	Unburned Hydro Carbons
WALE	Wall-Adapting Local-Eddy Viscosity

List of Symbols

$\tilde{E}$	Filtered Total Energy per Unit Mass
$\mathbf{f}_b$	Resultant of Body Forces
λ	Taylor Micro Scale
η	Kolmogorov Length Scale
ρ	Density
$\tilde{q}$	Filtered Heat Flux
$\mathbf{q}$	Heat Flux
σ	Stress Tensor
$\mathbf{T}$	Viscous Stress Tensor
$\tilde{T}$	Filtered Stress Tensor
$\mathbf{v}$	Continuum Velocity
Sm^3	Standard Cubic Meter
y^+	Dimensionless Wall Distance
u_τ	Friction Velocity
τ_w	Wall Shear Stress
ν	Kinematic Velocity
$\tilde{v}$	Filtered Velocity
$\bar{p}$	Filtered Pressure

Contents

1 Introduction

Regrettably, the combustion of crude oil continues to have an impact on the environment and human health. Climate change, acid rain and ocean acidifications continues to occur at concerning rates. Carbon dioxide (CO_2) and water vapor (H_2O) are the main products of crude oil combustion and increasing concentration of these products traps the radiation from the sun in the atmosphere, leading to an increasing average global temperature [1]. Other pollutants include nitrogen oxides (NO_x), sulfur oxides (SO_x), carbon monoxide (CO), unburned hydrocarbons and particulate matter (PM). It has been found that NO_x and SO_x react with water in the atmosphere, leading to harmful acid rains [2], as well as lowering overall air quality and depleting the ozone layer [3]. In large parts of the globe, environmental regulations have gradually become stricter to incentivize measures for reducing the negative impact of fossil fuel emission. However, applications in shipping, aviation and space technology still mainly require energy in a high density form. Transitioning to renewable energy sources is currently unfeasible in these areas and carbon-based fuels continue to dominate as the primary source. Despite being a fossil fuel, natural gas is an abundant resource located in underground reservoirs and has the highest energy density among the non renewables with respect to mass at $\approx$50MJ/kg [4]. It burns significantly cleaner than alternative fossil fuels in modern combustion systems and releases nearly negligible levels of SO_x and PM [5]. These properties make the use of natural gas a sensible alternative to fulfill the world's energy demand.

The purpose of a combustor is to convert chemical energy to kinetic energy. Combustors have evolved from a time when emissions were not considered at all, until today where the limitation of emission levels is the highest priority factor in the design. In the early life of the gas turbine combustors, fuel was not mixed with the oxidizer before combustion, leading to a diffusion flame. This gave a stable combustion process, but brought along very high emissions [6]. Nowadays, combustors use almost exclusively lean premix configurations, meaning that the reactants are mixed prior to entering the combustor and there is a surplus of air rather than burning at stoijchiometric conditions. Lean mixture is used with the intention of reducing the flame temperature and thus produce less NO_x. It is important that the mix between air and fuel is thorough to avoid zones in the combustion zone where the mix is less lean, which will lead to local hot zones with higher NO_x production [7]. The development of lean premix technology has awarded reduced emission levels, but lead to new challenges with flame stability, vibrations and mechanical

durability. These issues can have negative effects on the lifetime, efficiency and emission characteristics of the combustion system [8].

In this thesis, Siemens CFD software Star-CCM+ will be used to numerically analyze the combustion process in a lab-scale gas turbine combustor. The objective is to create a temperature and velocity profile and get an overview of the estimated emission levels. Large Eddy Simulation (LES) will be used as the turbulence model. LES is a transient technique where the scales larger than a given value are fully resolved in the flow domain, while the smaller scale motions are instead filtered and modelled. The filtering reduces the accuracy of the computation, especially in flows near walls or in multiphase flows. Every variable of the solution is decomposed into a filtered value and a sub-filtered value. Due to increasing computational power overall, the use of LES has become more common as of late. An advantage to modelling a smaller part of the turbulence and solving more of it is that errors in the assumptions of the model will have less impact on the solution. LES does not use time-averaged values and is thus always unsteady. To ensure that the large eddies can be captured, the mesh grid must be finer than the Taylor microscale, which is the length scale where viscosity significantly influences the eddies [9].

In the following chapter, the microturbine and combustor working principles are discussed. In the third chapter the concepts and governing laws behind combustion modelling are described. The simulation settings along with an experimental setup are described in chapter four, followed by the results in chapter five. In the sixth chapter, the computational results and experimental data are compared and discussed.

2 Background

2.1 Microturbines

Microturbines are relatively small gas turbines with power outputs between 20-500kW, which are typically used in low scale power generation applications. The turbines mainly consist of a compressor and a turbine on the same shaft, and a combustor. A recuperator may also be used to take advantage of the waste heat to improve the overall efficiency as well as reducing NO_x formation [10]. To achieve as high efficiency as possible, the tip of the turbine rotor blades should rotate close to the speed of sound [11]. Since microturbines have a relatively small total diameter, a high rotating speed is required. The operating speeds of microturbines may reach speeds close to 100000rpm [11]. As for all gas turbines, the microturbine works on the principle of the Brayton Cycle. In the first stage, air is compressed. Since all components use rotary motion, either axial-flow or centrifugal compressors are normally used. In the second stage, the fuel-gas is mixed together with the compressed air. The air-fuel mix is then burned in the combustor at constant pressure. This is called a premixed combustion. Due to the pressure being constant, the flame temperature becomes very high. Finally, the high pressure and temperature products powers the turbine. The high temperature is advantageous as it allows for a high Carnot efficiency limit, but at the same time demands a high temperature capacity of the turbine blades and leads to risks of forming undesirable products, like NO_x.

2.2 The Brayton Cycle

The gas turbine operates on the Brayton cycle with air being the working fluid. The cycle consist of four main processes.

a-b Adiabatic compression in the inlet.

b-c Constant pressure combustion of fuel.

c-d Adiabatic expansion in the turbine and exhaust. Extract work from the air to drive the compressor and the remainder for accelerating fluid.

d-a Constant pressure cooling of air back to initial conditions.

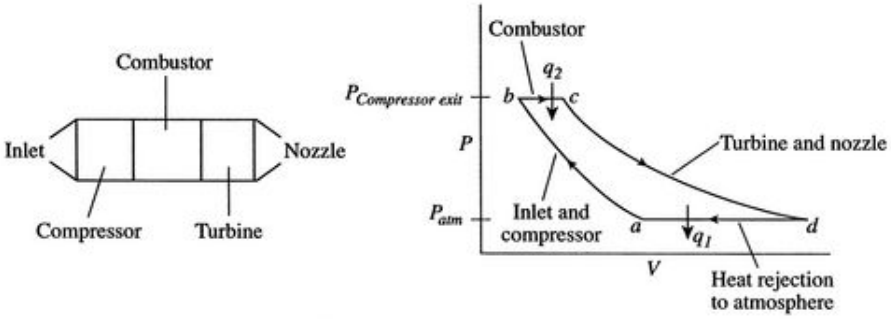

Figure 1: Jet engine components and thermodynamic states. Figure courtesy of MIT [12].

While the figure illustrates the ideal process, in reality, the process deviates slightly due to losses that affect the actual performance. Pressure loss occurs in the combustor due to turbulence. Turbulence is favorable to some degree as proper mixing between fuel and air is desirable. Excess turbulence is unfortunate however, as the losses become increasingly significant for the performance. Another source of pressure loss occurs due to the gas density decreasing with increasing temperature. The gas expands which in turn increases the velocity and momentum of the gas stream. The momentum change requires a force to be exerted on the gas stream and this force is provided by a pressure drop.

2.3 Natural Gas

Natural gas is an abundant resource located in reservoirs or sedimentary rocks below the earth's surface. The energy density of natural gas is the highest of the fossil fuels with respect to mass (≈50MJ/kg) [4]. It burns significantly cleaner than alternative fossil fuel in modern combustion systems. The gas normally stays trapped in permeable ground, but may be extracted by hydraulic fracking. Fracking is the process of pumping a fluid underground to induce cracks and movement in the ground, releasing the natural gas and making it available for extraction. The total volume of natural gas reserves worldwide has been estimated to 196.9 trillion Sm^3 (2018)[13]. In addition, the reserves are scattered over most parts of the globe [14], making it possible for nearly anyone to take advantage of the resource.

2.4 Combustor Performance Parameters

Among the most significant variables for overall performance there is the pressure loss throughout the combustor, combustion intensity and stability and outlet temperature profile. The overall efficiency is a direct measure of how complete the fuel is burned in the combustor. Ideally, 100% of the fuel should be burnt to minimize environmentally harmful emissions and maximize efficiency.

The efficiency is given by:

$$\eta_{combustion} = \frac{\delta h_{actual}}{\delta h_{theoretical}} = \frac{(\dot{m}_a + \dot{m}_f) + h_3 - (\dot{m}_a + \dot{h}_2)}{\dot{m}_f + LHV} \tag{1}$$

Where:
δh = change in enthalpy
h_2 = enthalply at compressor outlet
h_3 = enthalpy at turbine inlet
$\dot{m}_a$ = air mass flow rate
$\dot{m}_f$ = fuel mass flow rate
LHV = fuel lower heating / net calorific value

A big challenge when designing a combustor is handling the pressure loss caused by turbulence, skin friction and fundamental loss. It is impossible to eliminate the pressure loss completely, but a good benchmark is to limit the loss to 2-4% of the outlet pressure. Erosion and carbon deposits are other contributing factors to pressure loss [15]. The outlet temperature profile is another important consideration for the combustor design. It is beneficial to strive for temperature uniformity at the outlet to avoid high, local temperatures which can damage the turbine blades. To achieve better uniformity and lower temperature gradients, air film cooling and thermal barrier coating may be used.

Combustion intensity is a measure of heat release rate with respect to the size of the combustor. The heat release rate and combustion intensity is given by: When determining the size of the combustor, the required heat release is one of the most important parameters to consider. A larger volume allows lower pressure drops and higher efficiency and a more uniform temperature distribution. Closely related is the term combustion intensity, which is a measure of the ratio between the combustor size and rate of heat release [16].

$$\text{Nominal heat release} = m \cdot a \cdot AFR \cdot \text{fuel net colorific value} \tag{2}$$

Where: AFR = Mass air/fuel ratio

$$\text{Combustion intensity} = \frac{\text{heat release rate [kW]}}{\text{combustor volume} \cdot \text{pressure } [m^3 \cdot atm]} \quad (3)$$

2.5 Emission Control

During combustion, emissions of NO_x, CO and UHC should be minimized as far as practically possible. There are three main pollutants as a mechanisms contributing to the formation of NO_x. Thermal NO_x is NO_x which forms due to the high temperature during combustion. The amount of NO_x increases significantly when the flame temperature exceeds 1800K [17]. This mechanism is the highest contributor to NO_x emissions. In addition, some NO_x is formed due to nitrogen in the fuel reacting with oxygen in the combustor air. A third, less significant contributor is prompt NO_x which forms when atmospheric nitrogen reacts with hydrocarbon radicals.

Combustion at stochiometric conditions will lead to high formation of NO_x due to the gases reaching near adiabatic flame temperature. It is therefore common to take measures to reduce the flame temperature by lowering the air/fuel ratio, creating an excess amount of air. However, this will in turn increase the formation of CO and UHC due to incomplete combustion of fuel. Measures towards lowering the flame temperature must also consider the opposite effect [16].

Three main methods exist to lower emissions in gas turbines [6]:

1. Flame Temperature Reduction. Diluting the flame by injecting water or steam into the combustor.

2. Dry Low NOx. Mixing fuel and air prior to combustion with an excess amount of air (lean burn).

3. After-treatment. Selective catalyctic reduction may be used on the exhaust gases without having an impact on the combustion process.

3 Turbulent Combustion Modelling

Combustion is the process where a fuel or material is burned, leading to heat release and various concentrations of reaction products. As computational capatibility has become more powerful and widespread, the use of Computational Fluid Dynamics (CFD) has increased rapidly. Prototype and testing costs have decreased due to simulations becoming easier to perform with high accuracy. The goal with turbulent combustion modelling is to simulate the chemical reactions during combustion. This enables designers to create a temperature profile, predict emission levels during combustion and implement counter measures early in the design process [16].

3.1 Computational Approach

CFD uses numerical analysis to model fluid flow and is based on the governing equations of fluid mechanics. At the most basic level, the technique works by iterating the equations for conservation of mass, momentum and energy to arrive at a solution with a user-specified accuracy. When simulating a reacting flow, the fundamental Navier-Stokes equations for non-reacting flows may need a few additional terms to properly capture the chemical reactions. As opposed to for non-reacting flows, gas in reacting flows is non-isothermal. Heat capacity varies with varying temperature and fluid composition. The reaction rate needs to be taken into account. Since the gas always is a mixture, species diffusion and viscosity must also be considered. The following is a short description of the three main methods used for numerically solving turbulent flows.

A DNS or Direct Numerical Simulation solves the Navier-Stokes equations without taking any turbulence model into regard. All the spatial and temporal scales in turbulent flows are resolved. DNS requires a number of mesh points which scales largely with the Reynold's number[18]. Use of DNS is therefore mostly limited to flows with a low Reynolds number because it is very memory-intensive from a computational perspective, often making it impossible to use with hardware commonly available today.

The Reynolds-averaged Navier-Stokes (RANS) equations is another commonly used turbulence model for simulated flows. In this case the complete turbulence spectrum is simulated based on time-averaged values of the governing equation. The whole spectrum of fluctuations is averaged. RANS is

the least computationally expensive of the three methods, but also usually the least accurate.

Large Eddy Simulation (LES) is a turbulence model which saves computational expense by not solving the smallest length scales in the flow. This is possible due to low-pass filtering of the smallest eddies with lengths lower than a specified filter width. The smallest eddies are instead modelled by subgrid scales, with the Smagorinsky subgrid scale model being the most common. Since not all the length scales are solved, the accuracy of the model is lower than i.e DNS, especially in flows near walls or in multiphase flows.

While RANS has been widely used to simulate flows for many years, as availability of better hardware increases, it will in many cases make more sense to make use of LES or DNS for increased accuracy.

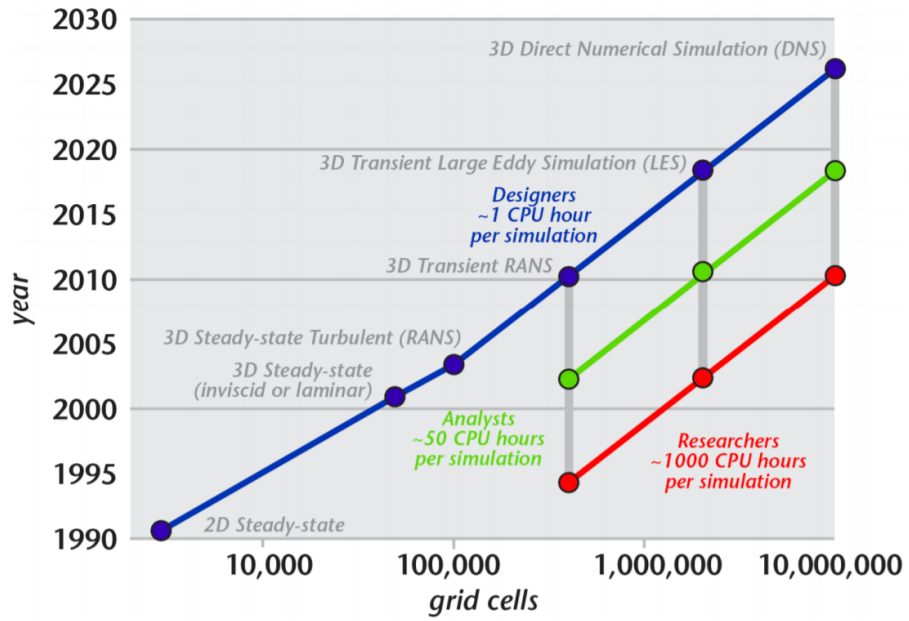

Figure 2: Evolution of computational power and turbulence models. Figure courtesy of Bakker CFD [19].

3.2 Siemens Star CCM+

The tool used for the numerical study of turbulent reacting flows is in this case the software Siemens Simcenter STAR-CCM+. STAR-CCM+ is capable of modelling a wide range of physical phenomena. Taking into account fluid mechanics, chemical reactions and heat transfer.

The software's mathematical models which describe the physics are all derived from fundamental conservation principles. An Eulerian implementation has been used, which means that the control volume represents a portion of space where material is allowed to flow [20]. The fundamental equations are presented in a differential form for an infinitely small control volume. However, these partial differential equations cannot be solved directly due to the total number of unknowns being higher than the number of equations. In order to solve these equations the various included terms need to be closed. To provide this closure the constitutive laws equations work as supplements to solve the partial differential equations. The software then used discretization to obtain a solution. The simulation domain is divided into a finite number of subdomains which are called cells. These cells collectively form a mesh. The mesh is generated by first populating the walls of the geometry, followed by growing the volumetric cells from the surface. The initial base layer is created by the Surface Remesher before the critical boundary layers are generated by the Prism Layer Mesher. The majority of the prism layer cells are of recangular shape, with variable size, aspect ratio and growth rate. Finally, the remaining volume mesh is populated by the Polyhedral Mesher [16].

3.3 Constitutive Laws

3.3.1 Governing Equations

The STAR-CCM+ software adapts the governing equations with some modifications from their original form. For turbulent reaction flow, which is the type of flow in this study, some of the fundamental Navier-Stokes equations need some additional terms to take into the account the chemical reactions. The adapted equations will be presented in this chapter and are taken from the handbook of STAR-CCM+. The most important differences are [21]:

- Reacting gas is non-isothermal. The software must track a mixtures of species individually and during the reactions the heat capacity varies along with changes in temperature and chemical composition.

- The reaction rate must be taken into account.

- Transport coefficients, like species viscosity and diffusion must be considered.

Conservation of Mass

The equation for conservation of mass is the same for a reacting flow as for a non-reacting flow. This makes sense as the combustion process neither creates nor discards any mass from the flow [6].

$$\frac{\delta \rho}{\delta t} + \nabla \cdot (\rho \mathbf{v}) = 0 \tag{4}$$

Where: ρ = density
$\mathbf{v}$ = continuum velocity

Conservation of Linear Momentum

The time rate of change of linear momementum is equal to the resultant force acting on the continuum [20].

$$\frac{\delta (\rho \mathbf{v})}{\delta t} + \nabla \cdot (\rho \mathbf{v} \otimes \mathbf{v}) = \nabla \cdot \sigma + \mathbf{f}_b \tag{5}$$

Where: $\otimes$ = tensor product (Kronecker)
$\mathbf{f}_b$ = resultant of the body forces
σ = Stress tensor

Conservation of Angular Momentum

Requires a symmetric stress tensor.

$$\sigma = \sigma^T \tag{6}$$

Conservation of Energy

The law of conservation of energy states that energy may only change form during a chemical reaction. No additional energy will be produced or wasted.

$$\frac{\delta(\rho E)}{\delta t} + \nabla \cdot (\rho E \mathbf{v}) = \mathbf{f}_b \cdot \mathbf{v} + \nabla \cdot (\mathbf{v} \cdot \sigma) - \nabla \cdot \mathbf{q} + S_E \tag{7}$$

Where: E = total energy per unit mass
q = heat flux
S_E = energy source per unit volume

The Star-CCM+ fluid flow solver has the ability to simulate internal and external fluid flow across a various range of flow regimes and types. When integrating the equations above over a finite control volume, the governing equations takes a different form [22].

Continuity equation:

$$\frac{\delta}{\delta t}\int_V \rho dV + \oint_A \rho v \cdot da = \int_V S_u dV \tag{8}$$

Where: t = time
V = volume
a = area vector
ρ = density
v = velocity
S_u = user-specified source term

Momentum equation:

$$\frac{\delta}{\delta t}\int_V \rho dV + \oint_A \rho v \otimes v \cdot da = -\oint_A pI \cdot da + \oint_A T \cdot da + \int_V f_b dV + \int_V S_u dV \tag{9}$$

Where: p = pressure
T = viscous stress tensor
f_b = body forces resultant
S_u = user-specified source term

Energy equation:

$$\frac{\delta}{\delta t}\int_V \rho E dV + \oint_A \rho H v \cdot da = -\oint_A q \cdot da + \oint_A T \cdot v da + \int_V f_b \cdot v dV + \int_V S_u dV \tag{10}$$

Where: E = total energy
H = total enthalpy
q = heat flux

3.3.2 Large Eddy Simulation

Large Eddy Simulation (LES) is a turbulence model which reduces computational expensive by neglecting the smallest length scales in the simulation, which normally would require most of the computational power. This is possible due to low-pass filtering of the smallest eddies with lengths lower than a specified filter width. The smallest eddies are instead modelled by sub-grid scales. However, this filtering technique reduces the accuracy of the model, especially in flows near walls or in multiphase flows. LES does not use time-averaged values, so it is always unsteady. To ensure that the large eddies can be captured, the mesh grid must be finer than the Taylor microscale. The Taylor microscale is the length scale where viscosity significantly influences the eddies [9].

The equations solved are achieved with a spatial filtering instead of an averaging process. The solution variable ϕ consists of a filtered value $\tilde{\phi}$ and a sub-filtered value ϕ

$$\phi = \tilde{\phi} + \phi' \tag{11}$$

Where: ϕ represents velocity components, pressure, energy or species concentration

The spatial filtering removes the smallest eddies and by doing so, the range of scales that needs to be resolved is reduced. The filtering of the generic instantaneous flow variable $\phi(t, x)$ is defined as [23]:

$$\tilde{\phi}(t, x) = \int \int \int_{-\infty}^{\infty} G(x - x', \Delta)\phi(t, x')dx' \tag{12}$$

Where: $G(x, \delta)$ = the filter function characterized by a filter width $\Delta = (\Delta_x \Delta_y \Delta_z)^{1/3}$

The smaller eddies are removed by the spatial filtering and with that the range of scales that needs to be resolved is reduced. LES filtering may be explicit or implicit. Explicit filtering means that a filter function (a box or Gaussian) is applied to the discretized Navier-Stokes equations. STAR-CCM+ uses implicit filtering, meaning that the computational grid determines the scales of the filtered eddies. Implicit filtering takes advantage of the grid resolution and thus achieves a less computationally expensive solver than its explicit filtering counterpart.

By inserting the decomposed solution variables into the Navier-Stokes equations, the filtered mass, momentum and energy transport equations becomes respectively:

$$\frac{\delta\rho}{\delta t} + \nabla \cdot (\rho\tilde{v}) = 0 \tag{13}$$

$$\frac{\delta}{\delta t}(\rho\tilde{v}) + \nabla \cdot (\rho\tilde{v} \otimes \tilde{v}) = -\nabla \cdot \tilde{p}I + \nabla \cdot (\tilde{T} + T_{SGS}) + f_b \tag{14}$$

$$\frac{\delta}{\delta t}(\rho\tilde{E}) + \nabla \cdot (\rho\tilde{v}\tilde{E}\tilde{v}) = -\nabla \cdot \tilde{p}\tilde{v} + \nabla \cdot (\tilde{T} + T_{SGS})\tilde{v} - \nabla \cdot \tilde{q} + f_b \tag{15}$$

Where: ρ = density
$\tilde{v}$ = filtered velocity
$\bar{p}$ = filtered pressure
I = identity tensor
$\tilde{T}$ = filtered stress tensor
f_b = resultant of the body forces (gravity and centrifugal)
$\tilde{E}$ = filtered total energy per unit mass
$\tilde{q}$ = filtered heat flux

The turbulent stress tensor now represents the subgrid scale stresses. The interaction between the larger, resolved eddies and the smaller, unresolved eddies causes these stresses. They are modeled using a Boussinesq approximation [23].

$$T_{SGS} = 2\mu_t S - \frac{2}{3}(\mu_t \nabla \cdot \tilde{v})I \tag{16}$$

Where: S = strain rate tensor

3.3.3 Subgrid Scale Turbulent Models

LES needs closure of the filtered Navier-Stokes equations. To achieve this, the subgrid scale stress tensor is modeled. This model provides a formula for the subgrid scale viscosity μ_t in the Boussinesq approximation of the subgrid

scale tensor [24]. Star-CCM+ has various options for subgrid scale models which may be used. For this simulation the WALE (Wall-Adapting Local-Eddy Viscosity) model was chosen. This is a modern subgrid scale model which uses a novel form of the velocity gradient tensor. It does suffer the shortcoming of containing a model coefficient C_s which is not universal and is dependent on local flow conditions. However, it has shown to seemingly be less sensitive to the value of this coefficient than the other common option, the Smagorinsky model. Another advantage of the WALE model is that it scales accurately at the walls and does not require any form of near-wall damping.

3.3.4 Wall Treatment

Vorticity is generated at the walls in most flows. For that reason it is essential to predict the flow across the wall boundary layer. The wall boundary layer describes the layer near a wall which is affected by viscosity. The velocity varies from zero closest to the wall, to the full velocity of the free stream. The normal distance from the wall to a point where the velocity is 99% of the free stream velocity is defined as the nominal thickness of the boundary layer. Viscous stresses further away from the wall than this point can be disregarded [25].

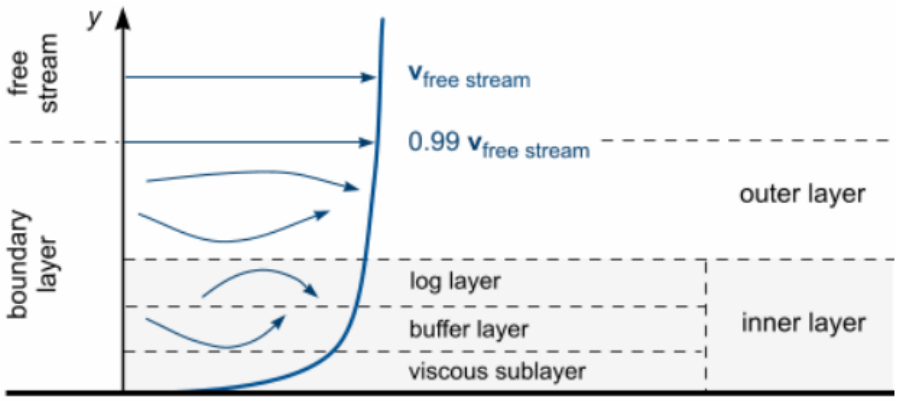

Figure 3: Velocity profile of turbulent flow boundary layer. Figure courtesy of Siemens [25].

- In the **Viscous Sublayer** the fluid is in contact with the wall. The viscous effects are dominant and the flow is almost laminar. The mean flow velocity in this region depends on the fluid's density, viscosity, wall shear stress and distance from the wall.

- The **Buffer Layer** is where the viscous sublayer transitions into the log layer.
- In the **Log Layer** the flow is dominated equally by viscous and turbulent effects.

For turbulent boundary layers, the physics must be modeled explicitly. For this simulation the All y^+ wall-treatment option was selected. Star-CCM+ calculates wall shear stress by the following equation [26]:

$$\tau_w = \rho u_\tau^2 \frac{\hat{v}_{tangential}}{|\hat{v}_{tangential}|} \tag{17}$$

By selecting All-y^+, the friction velocity becomes $\mathbf{u}_\tau = \mathbf{u}_*$.

Where the velocity scale $\mathbf{u}_*$ is calculated iteratively by equating $\mathbf{u}^+$ (eq. 18) with the wall-function definition for u^+ (eq. 19) [27]:

$$u^+ = \frac{u}{u_*} \tag{18}$$

Where: u = wall-tangential velocity component of the velocity vector
u_* = velocity scale representative of the flow velocity in the near-wall region

3.3.5 Segregated Flow Solver

The volume can be solved using either a segregated or coupled solution procedure. Using segregated methods, an equation for a given variable is solved for all cells, before moving on to the equation for the next variable in all cells, and so on. While with a coupled solver, a given cell quations for all variables are solved before the same process is repeated for all cells. The segregated flow solver is suitable for compressible flows at low Mach number [28].

3.3.6 Reacting Turbulent Flow

In simulations involving reacting flows, the conservation equation for energy is solved with the addition of the term accounting for heat release in the reaction [22].

Differential form:

$$\frac{\delta(\rho E)}{\delta t} + \Delta \cdot (\rho E v) = f_b \cdot v + \Delta \cdot (v \cdot \sigma) - \Delta \cdot q + S_E \tag{19}$$

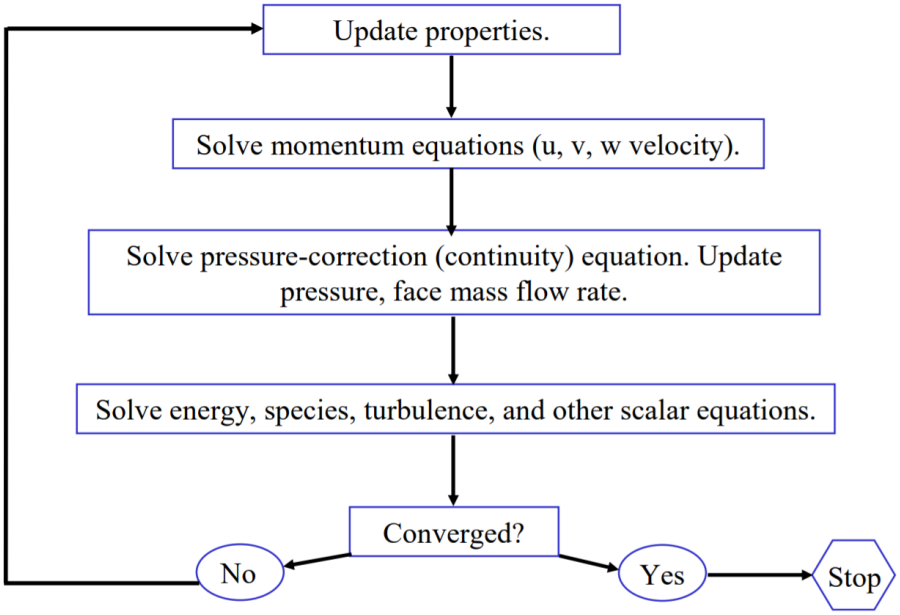

Figure 4: Segregated Flow Solver Process. Figure courtesy of Bakker CFD [28].

Integral form:

$$\frac{\delta}{\delta t}\int_V \rho E dV + \oint_A [\rho H v_r + v_g p]\cdot da = -\oint_A q''\cdot da + \oint_A T\cdot v da + \int_V f_b v dV + \int_V S_E dV \tag{20}$$

Where: S_E = source term

In addition, the conservation equations for species mass fractions (Y_i) are solved with the following equations:

Differential form:

$$\frac{\delta \rho Y_i}{\delta t} + \Delta\cdot(\rho U Y_i) = \Delta\cdot(J_i + \frac{\mu_t}{\sigma_t}\Delta Y_i) + S_{Y_i} \tag{21}$$

Integral form:

$$\frac{\delta}{\delta t}(\int_V \rho E dV + \oint_A [\rho H v_r + v_g p]\cdot da = -\oint_A q''\cdot da + \oint_A T\cdot v da + \int_V f_b v dV + \int_V S_E dV \tag{22}$$

Where: S_{Y_i} = mass fraction source term from reactions

4 Simulation Setup

4.1 Geometry

The combustor was designed and modelled as part of a Bachelor's thesis by students at Western Norway University of Applied Sciences in 2017. A further description of the design choices and assembly can be found in chapter 4.12. In order to save computational expense, unnecessary details of the model were supressed prior to importing it into STAR-CCM+. Exterior parts like the flanges, sensors and plugs would not have an impact on the simulation and were therefore removed. Sharp edges and gaps which would not have any, or minor, effects on the results were also removed or filled wherever applicable. The final geometry was imported into STAR-CCM+ as shown below.

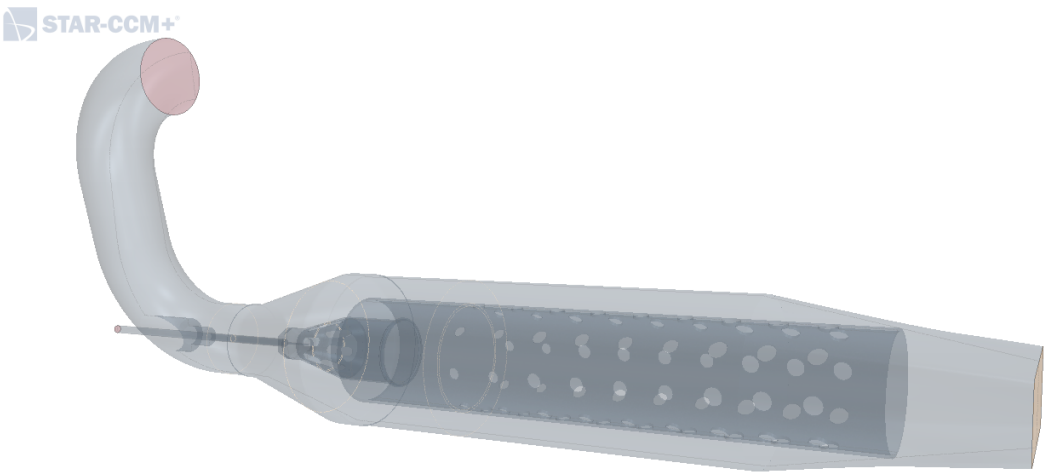

Figure 5: Combustor model geometry imported into STAR-CCM+.

4.2 Physics

Active physics model were selected as shown in table below. Default values were used for any parameters which are not included in the list.

Parameter	Enabled Model
Space	Three Dimensional
Time	Implicit Unsteady
Material	Multi-Component Gas
Reaction Regime	Reacting
Reacting Flow Models	Flamelet
Flamelet Models	Steady Laminar Flamelet
Turbulence	Large Eddy Simulation
Flow	Segregated Flow
Enthalpy	Segregated Fluid Enthalpy
Equation of State	Ideal Gas
Viscous Regime	Turbulent
Subgrid Scale Turbulence	WALE Subgrid Scale
Gradient Metrics	Gradients
Wall Distance	Exact Wall Distance
LES Wall Treatment	All y^+ Wall Treatment
Flame Type	Non-Premixed Flame
Energy Option	Non-Adiabatic
Optional Models	Cell Quality Remediation
Optional Models	NO_x Emission
Specific NO_x Models	NO_x Thermal
Thermal NO_x Models	NO_x Zeldovich

Table 1: Physics Continuum Models

The inlet air was treated as an ideal gas during this simulation. Cell Quality Remediation was an optional function which was activated with the purpose of helping to find a solution in parts where the mesh is sub-optimal. The model identifies poor-quality cells using a set of predefined criteria. Once these cells are marked, the computed gradients in the cells are modified in a way to improve the robustness of the solution [29]. The remaining selected models will be described in the following sub chapters.

4.3 Initial Conditions

The initial conditions should preferrably be set in a way so that they are not too far from the expected results. The table below described the modified parameters for the initial conditions. The parameters which are not mentioned are set to default values.

Parameter	Value	Note
Mixture Fraction Profile	0.0	Pure oxidizer
Mixture Fraction Variance	0.0	
Pressure	101325 Pa	Atm
Static Temperature	300 K	Ambient
Turbulence Intensity	0.0	No turb. initially
Turbulence Length Scale	0 m	No turb. initially
Velocity	0.0, 0.0, 0.0	No vel. initially

Table 2: Initial Conditions

4.4 Boundary Conditions

Suitable initial and boundary conditions are mathematical components which are mandatory in order to solve the necessary equations. The boundary conditions determine the direction of the flow and which parts of the model are fluid and solid. There are various types of boundary types to select between in STAR-CCM+. In this simulation, mass flow inlets and a standard outlet was used as they closely replicate the actual combustor conditions. All walls in the simulation domain are adiabatic with no heat transfer through the walls. One method for specifying the turbulence parameters is to specify the turbulence intensity and length scale.

The turbulence intensity is defined as:

$$I = \frac{\sqrt{\frac{2}{3}k}}{u} \tag{23}$$

Where: $k =$ turbulence kinetic energy
$u =$ local velocity magnitude

The initial condition values are taken from one of the experimental setups performed on the same combustor in 2019, which are described further in chapter 4.12. The parameters which are not listed are set to default values in STAR-CCM+.

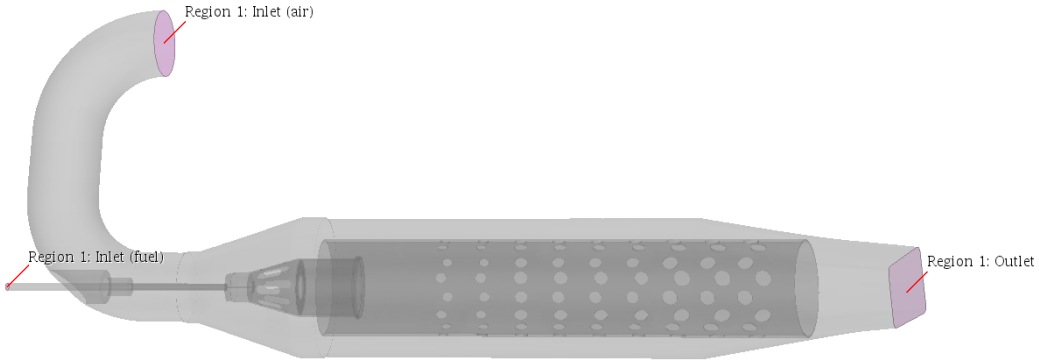

Figure 6: Inlets and outlet.

Air Inlet Boundary Conditions

Parameter	Value	Unit	Note
Type	Mass Flow Inlet	-	-
Mass Flow Rate	0.0699	kg/s	
Mixture Fraction Profile	0.0	-	Pure oxidizer
Supersonic Static Pressure	105325	Pa	
Total Temperature	300	K	-
Turbulence Intensity	0.05	-	-
Turbulence Length Scale	$3.6 \cdot 10^{-3}$	m	-

Table 3: Air Inlet Boundary Conditions

Fuel Inlet Boundary Conditions

Parameter	Value	Unit	Note
Type	Mass Flow Inlet	-	-
Mass Flow Rate	$8.09 \cdot 10^{-4}$	kg/s	
Mixture Fraction Profile	1.0	-	Pure fuel
Supersonic Static Pressure	201325	Pa	
Total Temperature	300	K	-
Turbulence Intensity	0.05	-	-
Turbulence Length Scale	$3.15 \cdot 10^{-4}$	m	-

Table 4: Fuel Inlet Boundary Conditions

Outlet Boundary Conditions

Parameter	Value	Unit	Note
Type	Outlet	-	-
Split Ratio	1	-	One outlet only

Table 5: Outlet Boundary Conditions

4.5 Determining Cell Size

A preliminary RANS simulation was run to find the Kolmogorov Length Scale and Taylor Micro Scale values.

Scale	Minimum	Maximum
Kolmogorov Length Scale [m]	$1.4986{\cdot}10^{-6}$	$2.3053{\cdot}10^{-4}$
Taylor Micro Scale [m]	$1.9536{\cdot}10^{-5}$	$5.5476{\cdot}10^{-4}$
Kolmogorov Time Scale [s]	$2.4672{\cdot}10^{-7}$	$1.1768{\cdot}10^{-3}$
RANS Model Base Cell Size	-	-

Table 6: Length and Time Scales

The Kolmogorov Length Scale η and the Taylor Micro Scale λ are used to determine a reasonable cell size for the LES simulation, where $\eta < \Delta < \lambda$. Given the Taylor Micro Scale values, the average cell size should preferrably be 0.55mm or lower. However, hardware limitations made it difficult to generate a mesh with a smaller base size than 0.6mm.

4.6 Prism Layers

To adequately capture the flow behaviour near the wall, the mesh adjacent to the wall should be fine enough to capture the boundary layer flow. This part of the mesh consists of prism layers which in total should be equal to or higher than the boundary layer. The universal law of the wall states that the velocity distribution close to the wall is similar for almost all turbulent flows [30]. One of the most important parameters when describing the wall function is the the dimensionless wall distance y^+, which is given by:

$$y^+ = \frac{yu_\tau}{\nu} \tag{24}$$

Where: y = the absolute distance to the wall
u_τ = friction velocity
ν = kinematic velocity

For wall-resolved LES, the first cell height should be within the viscous sublayer of the boundary layer ($y_0^+ < 5$) [31]. After the first layer, a growth factor is set to change the increase of height between each boundary layer

element h. The factor is always greater than 1 because tighter mesh spacing is needed close to the wall. Ideally the final layer should be equal to the size of the mesh in the unstructered region, creating a smooth transition [31]. In general, prism layer stretching above 1.4 is considered too large to accurately capture the boundary layers. A stretching value below 1.2 carries the risk of generating more elements than necessary. It is impossible to know the exact proper y^+ before running the first simulation, because the value is dependent of the local fluid velocity which in most cases will vary significantly across the wall. For that reason a trial and error method was used to find a decent y^+ value. In this simulation the Wall Thickness mode was activated to be able to choose the height of the first and most significant prism layer. If the y^+ value is too large, the first layer height may be reduced using this parameter.

4.7 Mesh

The density of the mesh should be sufficiently high to capture all the relevant features of the flow. Meshers used in this simulation were the Surface Remesher, Polyhedral Mesher and the Prism Layer Mesher. The polyhedral mesher is beneficial for geometries that involves a lot of curves and gaps across small areas. Although a finer mesh would be preferrable, issues started occurring with the mesher when attempting a base size lower than 0.6mm. The parameter settings which are not mentioned remained as default values. The total generated volume mesh consisted of 25 million cells.

Parameter	Value
Base Size	0.6mm
Target Surface Size	100% of base
Minimum Surface Size	10% of base
Surface Growth Rate	1.3
Number of Prism Layers	7
Prism Layer Near Wall Thickness	0.1mm
Prism Layer Total Thickness	3mm

Table 7: Global Mesh Settings

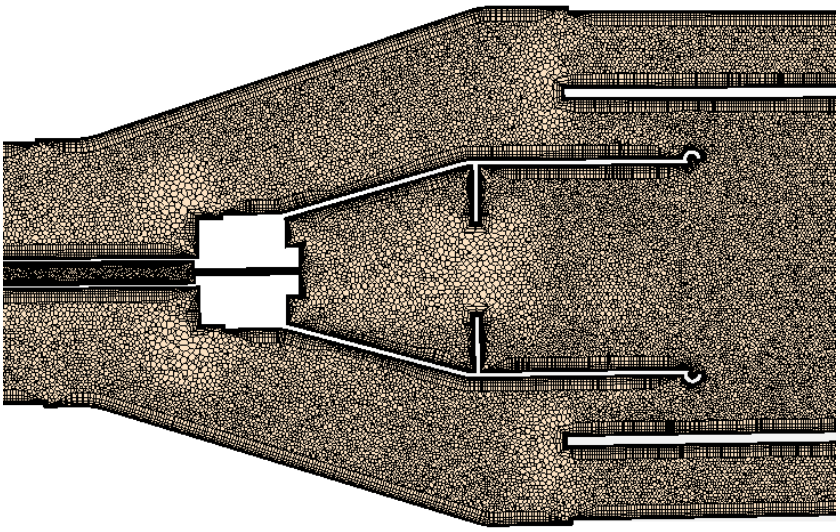

Figure 7: Vertical plane mesh sample

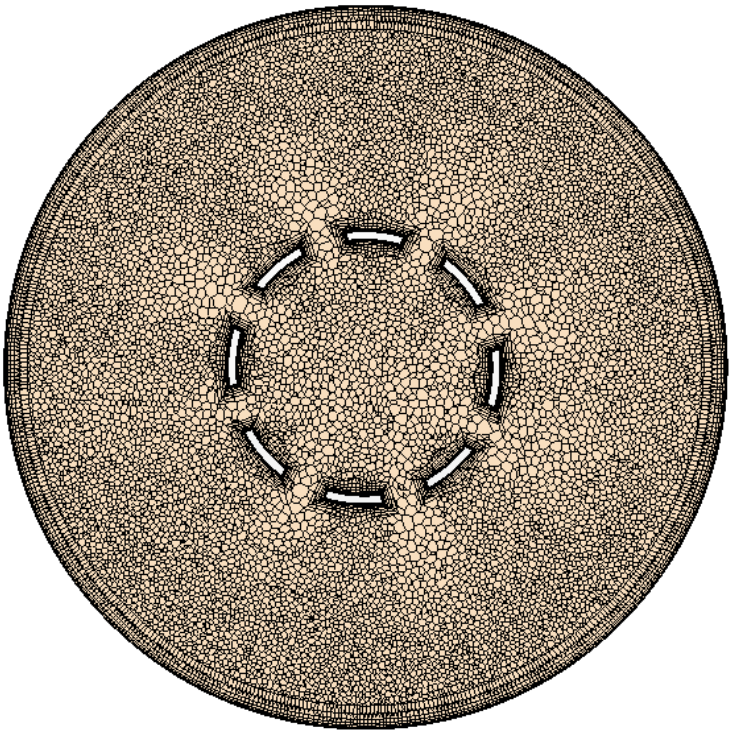

Figure 8: Horizontal plane mesh sample

4.8 Flamelet Methods

In this simulation the Steady Laminar Flamelet (SLF) Method was selected as this is suitable for cases where the oxidizer and fuel are supplied through seperate lines into the combustor. Using this method, the combustion becomes a function of the mixing fraction (Z) and a probability density function (PDF). The SLF method parameterizes all of the species in a chemical mechanism by reaction progress, mixture fraction and enthalpy. The sum of all involved species always equals one. The ignition that occurs when starting the combustion process does not exist in the SLF method. Combustion is solely represented by the function of mixture fraction and variance. In a numerical model no igniter is necessary. The SLF table for this simulation was generated with 101 mixture fraction grid points and 19 mixture fraction variance grid points.

4.9 Reactions

The chemistry effects upon combustion are stored in the SLF table which is generated in STAR-CCM+. The chemical mechanism files were acquired from the University of California San Diego library of Chemical-Kinetic Mechanism for Combustion Applications [32]. The chemistry is designed to focus on conditions relevant to flames, ignition and detonations at high temperature. The number of species and reactions are kept to a minimum necessary to describe the systems in order to reduce the uncertainties in the rate parameters as much as possible.

Fluid Chemistry Reaction File: *sandiego*20161214_*mechCK.txt*.

Fluid Thermodynamics Properties File: *sandiego*20160815_*therm.txt*.

The fuel composition in the SLF Table Generator was set to 100% C_3H_8 with a temperature of 300K. The oxidizer consisted of 23.3% O_2 and 76.7% N_2, with a temperature of 380K.

4.10 Hardware

Running a simulation with STAR-CCM+ is mainly CPU and memory demanding. The simulation in this work was run on a computer with the following specifications.

Component	Specification
CPU	Intel Core i5-9600 6-core 3.7/4.6GHz
RAM	Corsair DDR4-2666MHz C16 BK DC 32GB

Table 8: Hardware Specifications

4.11 Solvers

Due to hardware limitations, a time step of 1ms was chosen for this simulation. Larger time steps was avoided to reduce the risk of divergence or an inaccurate solution. For each time step, the default value of 15 inner iterations was selected. In order to help achieve convergence, a 1st-order Temporal Discretization was selected, slightly reducing the solvers accuracy as a consequence.

4.12 Experimental Setup

In this section the development process of the combustor will be described. It was tested in a small-scale gas turbine using propane gas fuel. The design choices and experimental setup will be described along with the test results. The objective of the experiment was to measure the temperature distribution of the combustor and map the emission levels in different configurations. Another goal was to achieve a complete combustion with as low concentration of unburned hydrocarbons as possible. The gas turbine used in the experiment was designed and assembled by groups of students at the Western University of Applied Sciences in 2017. It has gone through a series of changes and modifications, with the latest prior to these tests being a completely new combustor, which will be described in more detail in the following section.

4.12.1 Combustor Design Details

The high temperature caused by combustion, pressure variation and vibration are all factors that increase the risk of cracks developing in the combustor liner or nozzle. The edges of the liner holes are critical points due to stress concentrating in these areas, as well as rapid changing temperature which may lead to thermal fatigue. These considerations need to be taken into account in addition to the goal of reducing emissions to the lowest level possible. The combustor was designed mainly based on recommendations found in literature. Most of the design choices will be explained in further detail.

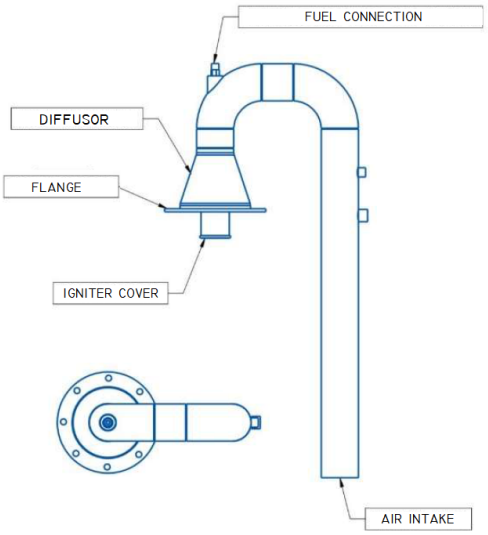

Flow of air was fed from the top, following examples in relevant literature[15]. This should prevent an uneven flame distribution. Between the air intake and the combustor there is a diffusor, with the purpose of reducing the velocity of the flow. The air velocity needs to be lowered prior to entering the combustor, to prevent the flame from being extinguished. The pipes, flanges and diffusor are all in AISI316L stainless steel material, due to its ability to withstand high temperatures. The casing was di-

mensioned based on the compressor's suction pipe diameter. According to [15], the diameter of the casing should be 2.1 times larger than the suction pipe of the compressor. Therefore the casing diameter was calculated to be:

D_{casing} = 2.1 x D_{pipe} = 2.1 x 55 = 115.5mm.

Due to limited availability of exact sized pipes, a 114.3mm (4") pipe was acquired and used as a casing. The length of the casing is based on a recommendation from the same source, which states that the length should be 2-4 times the casing's diameter. Based on that, the length of the casing was chosen to be 450mm. Similarly as for the casing, the flametube's diameter is also dimensioned with respect to the compressor's suction pipe diameter. The recommended ratio is 1.3 [15].

$D_{flametube}$ = 1.3 x D_{comp} = 1.3 x 55 = 71.55.

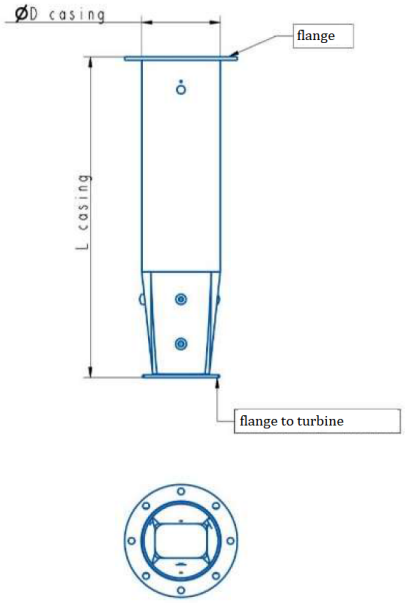

(a) Figure 3: Casing

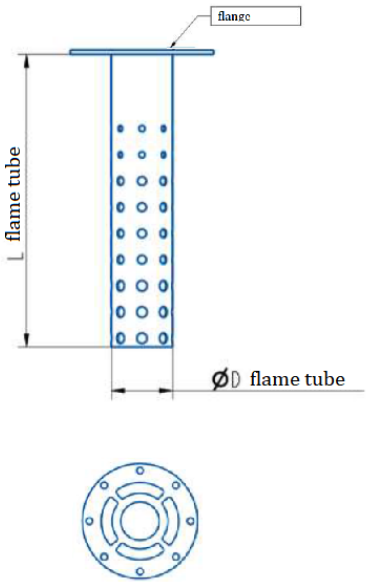

(b) Figure 4: Flame Tube

Industry standard pipes are not available in all sizes, so for practical reasons a 76.1mm (2 1/2") pipe was used. The casing length is recommended to be 3-6 times the length of the flame tube diameter and was therefore determined

to be 375mm[15]. There are 4 gaps on the flange of the flame tube for cooling air to pass through. The bypassing cooling air is not meant to enter the combustion zone, but has the purpose of diluting the combustion flame. This will reduce the temperature and reduce NO_x formation. According to the Gas Turbine Engineering Handbook, there should be 80 holes distributed over 10 rows for good efficiency[15]. Scaled with respect to liner diameter, the diameter of the holes should vary between 8, 10 and 12mm. The sizing of the holes in the dilution zone may be manipulated in order to achieve a desired temperature profile. Based on experience, the top row of holes was neglected because a large part of the primary air enters the combustion zone through the injector anyway. More air entering the combustion zone could have diluted the air/fuel mixture excessively, making it difficult to maintain a stable flame.

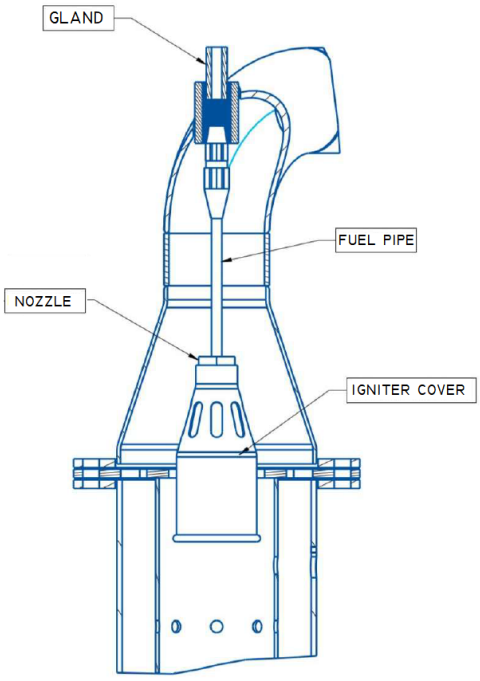

The igniter was chosen following the recommendation by a local company (Gasservice AS), who are specialized on propane equipment. It was mounted at the center of the flame tube as shown in the illustration. The igniter cover contributes to maintaining a more stable flame.

Exhaust gas measurement is a complicated field. In this experiment, an advanced gas analyzer called Horiba PG 350E was used. It is a device capable of measuring concentrations of NO_x, SO_2, CO_2, CO and O_2. To get more accurate values, the exhaust gas leaving the combustor was dried using a specialized dryer. A method called chemiluminescence was used to measure NO_x. When common air pollutants react, there is a resulting light emission [33]. Chemiluminescence takes advantage of this phenomenon and converts the intensity of the emitted light into a readable value. When NO reacts with oxygen and forms NO_2 the device measures the emitted light and provides a value for the NO_x concentration.

4.12.2 Test Setup

A cold test was initially performed to measure the pressure loss in the system. Without fuel flowing in the system, turbulence will be lower and thus a more accurate value for pressure loss can be found.

The experiment was performed with varying fuel pressure. During the hot test propane was supplied into the combustor and ignited. Temperature, inlet pressure and exhaust gas was measured. Unfortunately, due to high

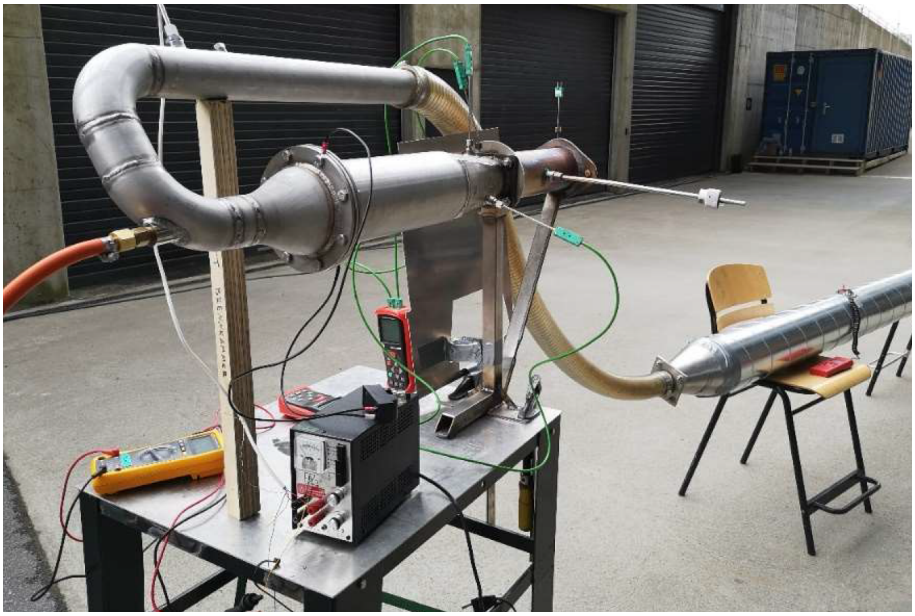

Figure 10: Test Setup

turbulence, pressure at the combustor outlet could not be measured accurately with equipment on-hand. Propane was used as test fuel. In order to ignite the combustor, the air fan was started at low speed just to get sufficient air for the propane to react. To avoid accumulation of propane inside the combustor, the igniter was turned on prior to opening the fuel supply. Propane and air supply rate was gradually increased until a stable flame was achieved. To measure the fuel consumption the propane tank was weighed at given time intervals during each test.

4.12.3 Assumptions

Some assumptions were made for the practical experiment:
- Air is incompressible at low speed (Ma < 0.3).
- The exhaust gas is treated as dry.
- Homogenously mixed exhaust gas due to turbulence.
- Stagnation pressure at the compressor outlet is the same as the stagnation pressure in the ventilation pipe.
- The mass flow of propane is constant when the pressure is constant.
- The mass flow of air and propane is 0.3 kg/s through the combustor.
- Stochiometric air fuel ratio is 15.6 kg air per kg fuel.

4.12.4 Measuring Points

Three temperature sensors were placed right below the flame tube. Another temperature sensor was placed at the inlet and another at the outlet. At the combustor inlet there is a pressure sensor to measure the inlet pressure, P2. Because of turbulent flow at the compressor outlet, the pressure sensor is placed as near to the top as possible. Nevertheless, it needed to be located before the elbow connections to minimize pressure drop. At the outlet of the combustor the flow had both a high velocity and temperature, which made it impractical for placing a sensor. Measurements at the outlet would only be performed during the cold test, to measure pressure drop through the combustor.

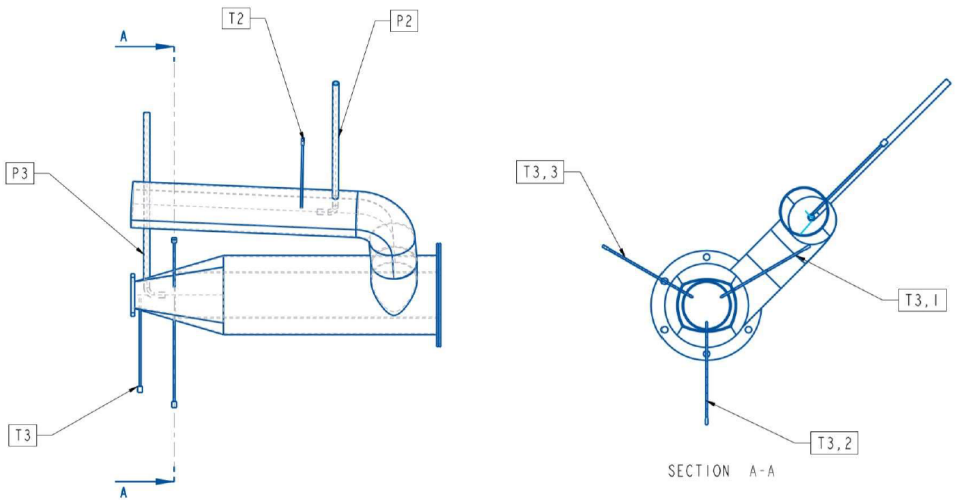

(a) Side View (b) Top View

Figure 11: Measuring Points

5 Results and Discussions

5.1 Results of Simulation

The simulation ran for a total of 220 hours. The CPU ran continuously at 4.3GHz, consuming an average of 28GB of memory. After visually inspecting the temperature and mass fraction of fuel, it was determined that convergence had been reached after approximately 5000 iterations. Equalling a physical flow time of: 5000 iterations x 1ms / 15 inner iterations = 330ms.

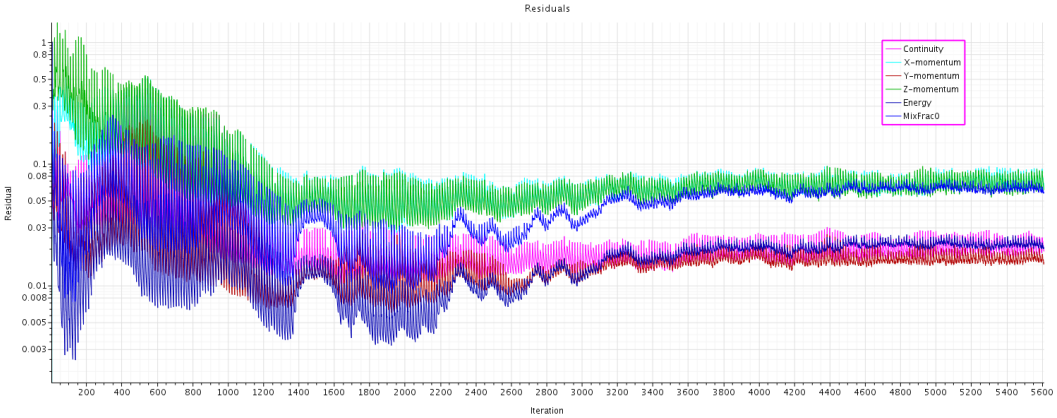

Figure 12: Residuals

5.1.1 Scalar Points

To make the results easier to read, a cross section scalar plane and a probe lines was generated at the swirler, flametube and outlet respectively. In an attempt to validate the results by comparing the experimental temperature measurements and the simulation, measuring points T3_1, T3_2, T3_3 as illustrated in figure 11, were recreated as probe points in the model geometry.

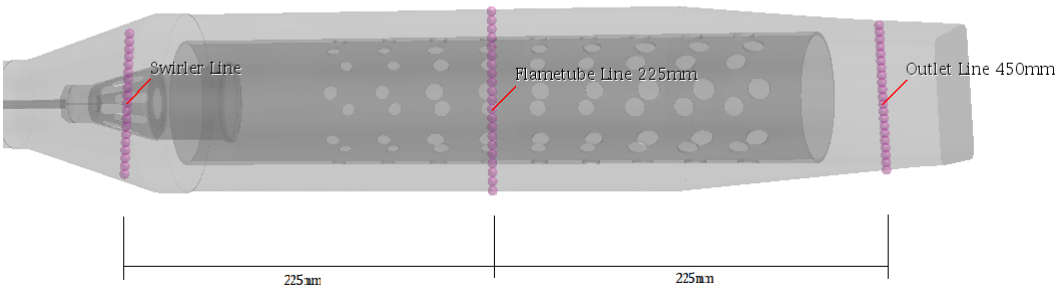

Figure 13: Horizontal cross section probe lines

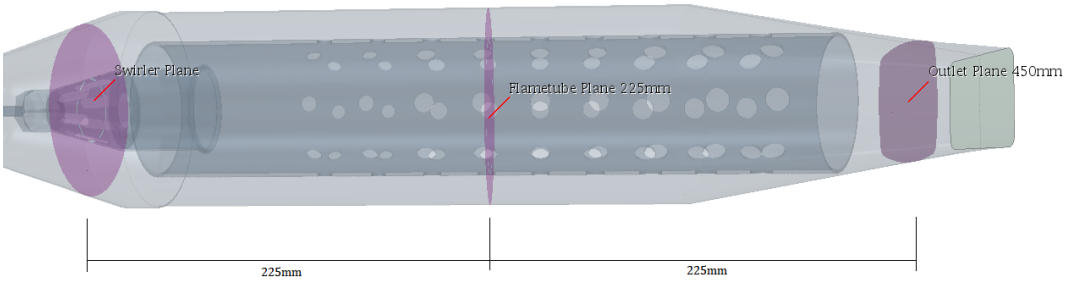

Figure 14: Horizontal cross section scalar planes

5.1.2 Converged Values

Parameter	Location	Min	Max	Unit
Absolute Pressure	Swirler	203.80	203.80	kPa
Absolute Pressure	Flametube	203.85	203.86	kPa
Absolute Pressure	Outlet	203.60	203.90	kPa
Temperature	Swirler	300.53	2241.90	K
Temperature	Flametube	367.06	2150.50	K
Temperature	Outlet	307.99	2211.90	K
Velocity	Swirler	0	96.66	m/s
Velocity	Flametube	0	29.06	m/s
Velocity	Outlet	0	21.18	m/s
Mass Fraction C_3H_8	Outlet	0	0	-
Mass Fraction CO	Outlet	0	0.163	-
Mass Fraction CO_2	Outlet	0	0.154	-
Mass Fraction N_2	Outlet	0.680	0.767	-
Mass Fraction O_2	Outlet	0	0.232	-

Table 9: Converged Values

5.1.3 Temperature Profile

Below are the temperature distributions shown in the vertical and horizontal plane cross sections.

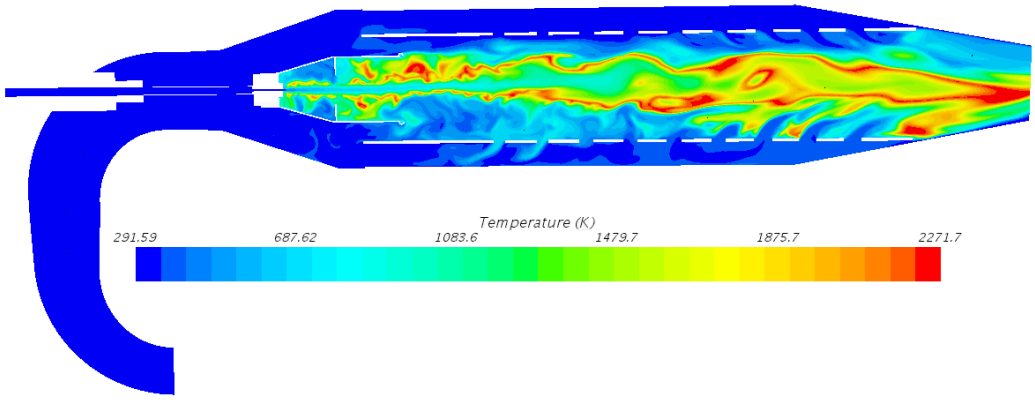

Figure 15: Vertical plane section temperature profile

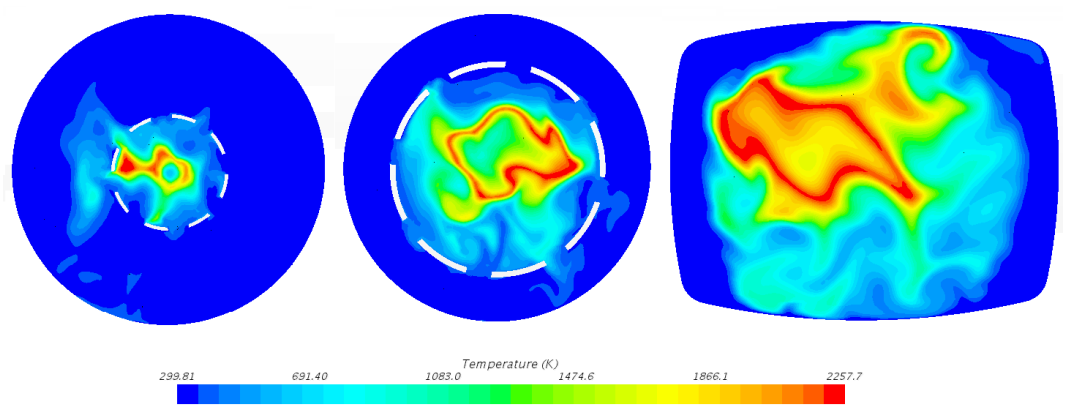

Figure 16: Horizontal plane section temperature profiles of swirler (left), flametube (middle) and outlet (right).

The converged temperature value at measuring points T3_1, T3_2 and T3_3 were 1275K, 620K and 2050K respectively.

5.1.4 Velocity Profile

The fuel enters the combustor at high velocity, staying well-centered throughout the whole flametube and outlet. Air enters through the air inlet and has a skewed velocity profile with higher velocity at the top compared to the lower part.

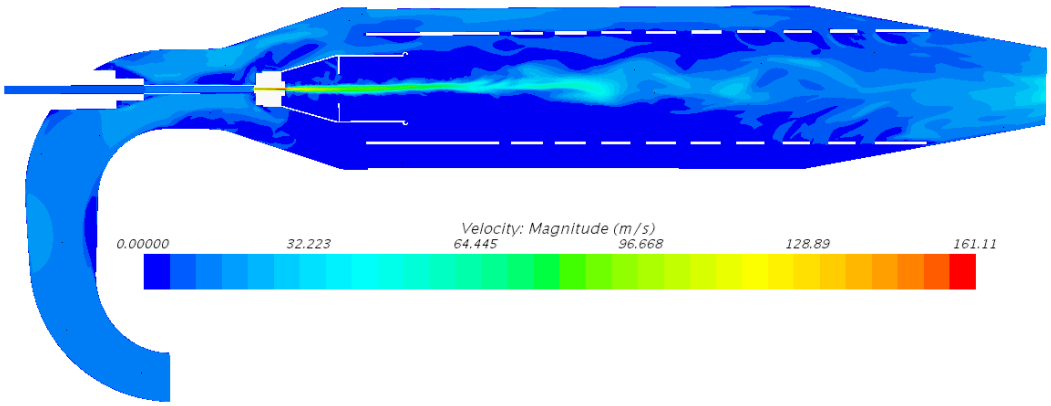

Figure 17: Vertical plane section velocity profile

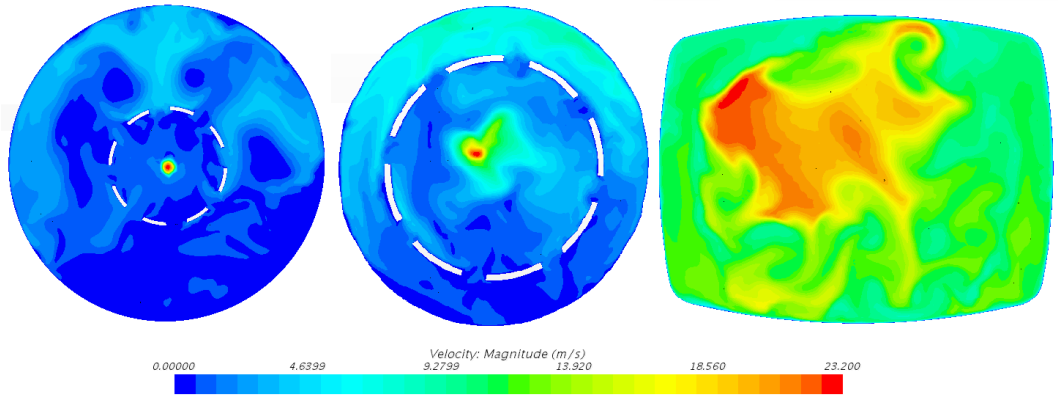

Figure 18: Horizontal plane section velocity profiles of swirler (left), flametube (middle) and outlet (right).

5.1.5 Turbulent Length Scale

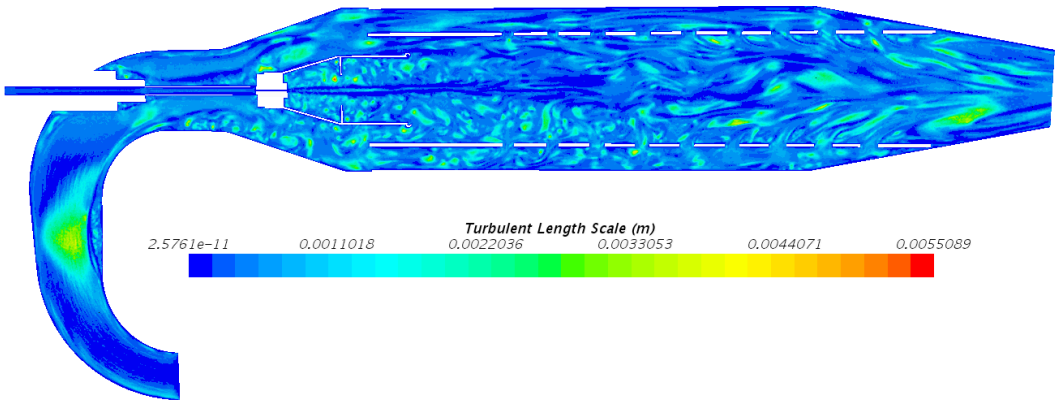

Figure 19: Vertical plane section turbulent length scale L_t

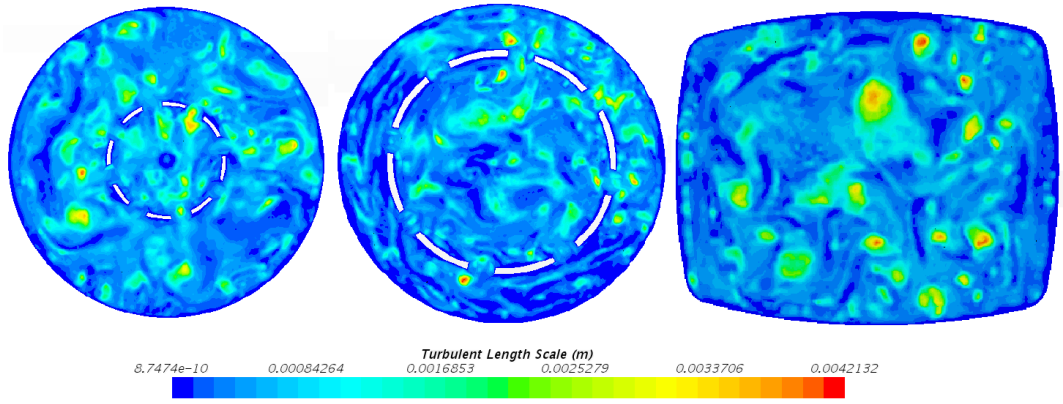

Figure 20: Turbulent length scale L_t across swirler (left), flametube (middle) and outlet (right).

5.1.6 Mass Fraction of Species

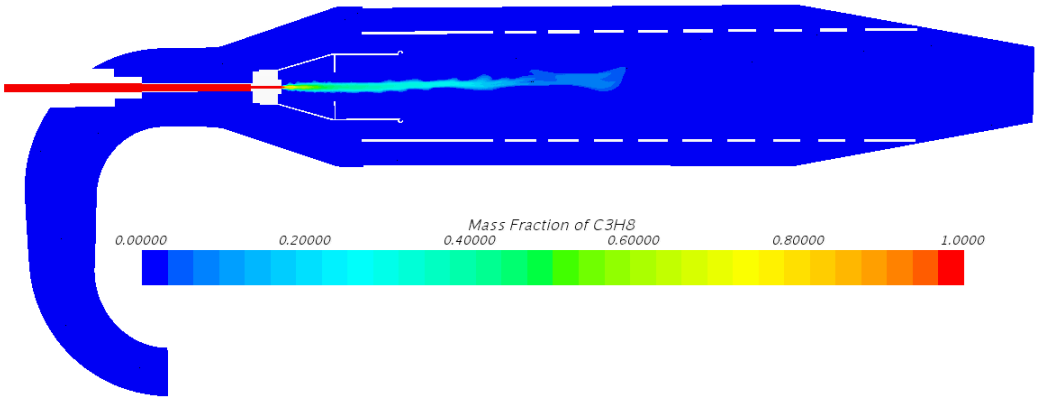

Figure 21: Mass Fraction of C_3H_8

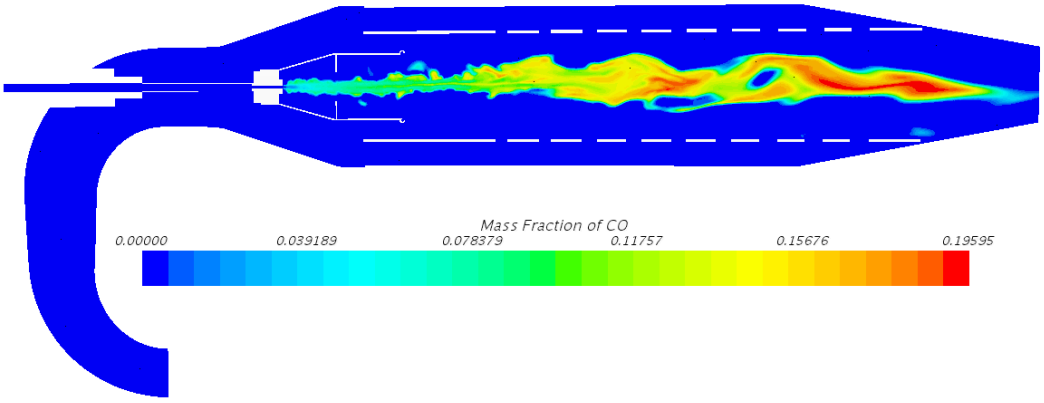

Figure 22: Mass Fraction of CO

To find values for NO_x emissions, a second simulation was run with larger time steps (2ms) and fewer inner iterations per time step (5). This was due to the NO_x model not being active on the initial simulation. By default, only one source of NO_x may be enabled in STAR-CCM+ at a given time. In this instance, the thermal NO_x model was selected since it would be the main cause of NO_x emissions created in this combustion process.

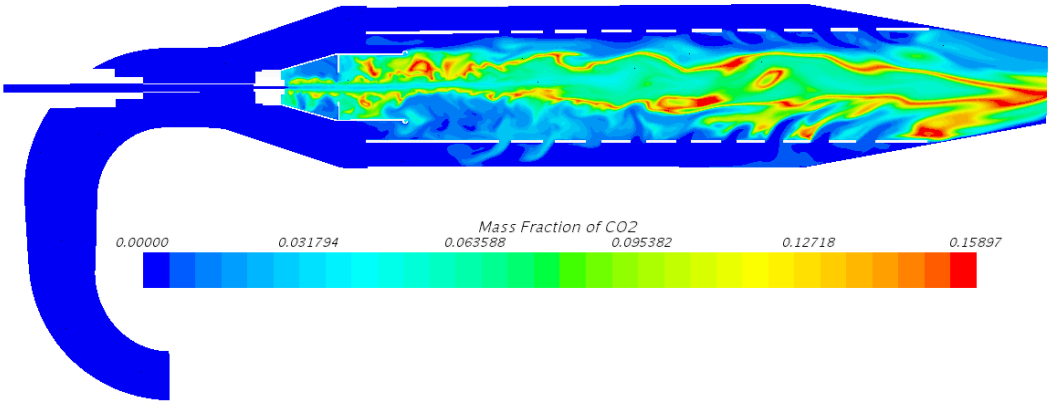

Figure 23: Mass Fraction of CO_2

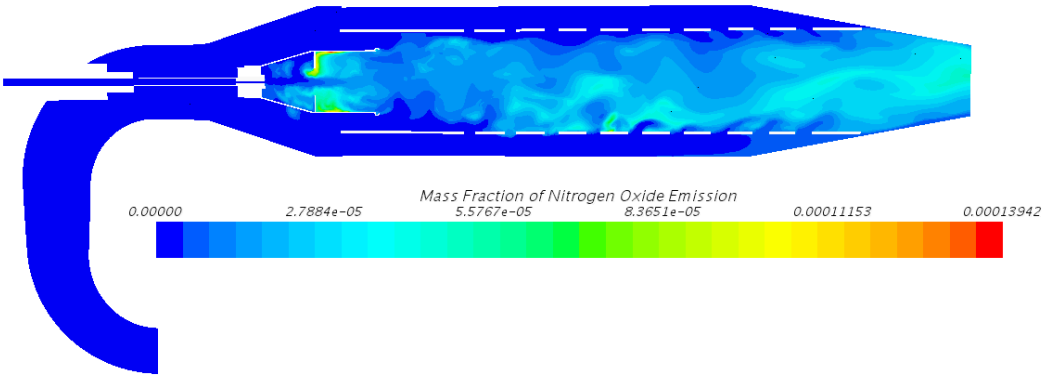

Figure 24: Mass Fraction of NO_x

5.1.7 Solution History

The simulation was halted and saved for every 50ms equivalent physical time. Values for temperature, velocity, mass fraction of fuel and turbulent length scale L_t were exported at these time steps and plotted for the respective scalar cross section planes. The inputs in the plots are average and/or maximum values in the respective locations at the given point of time. The plots are interpreted in the next chapter.

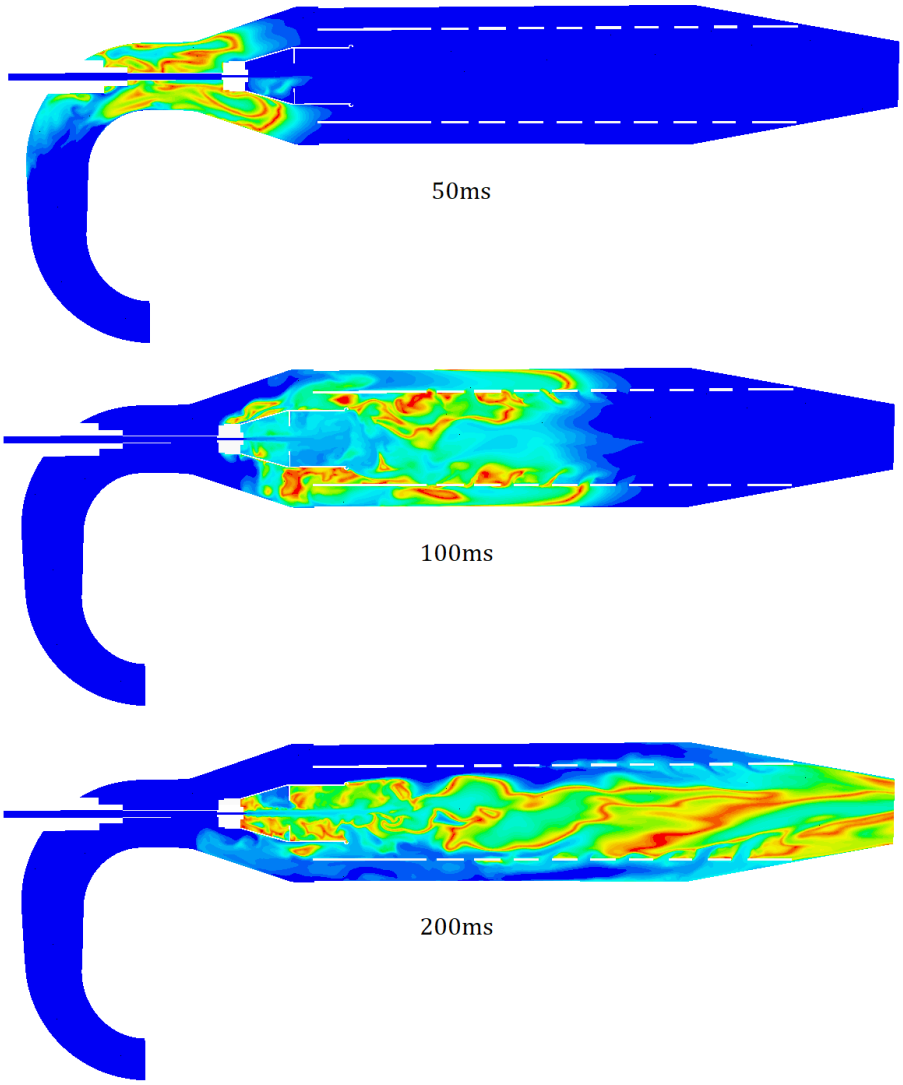

Figure 25: Temperature distribution change over time

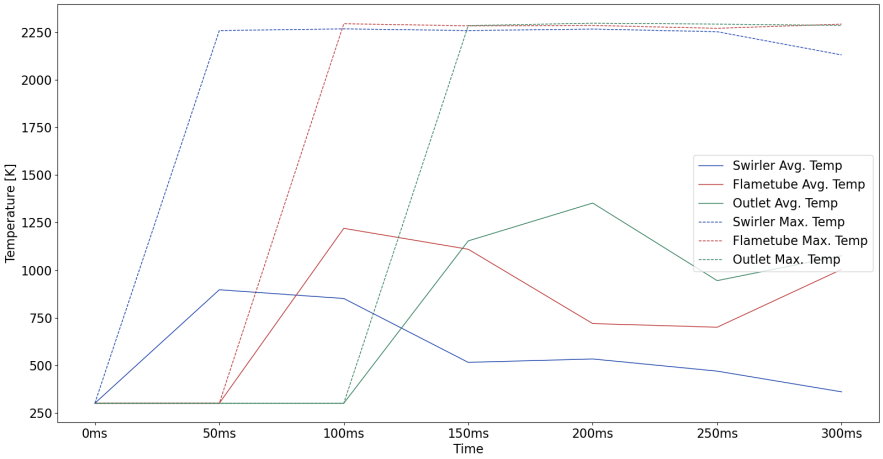

Figure 26: Average and Maximum Temperature over Time

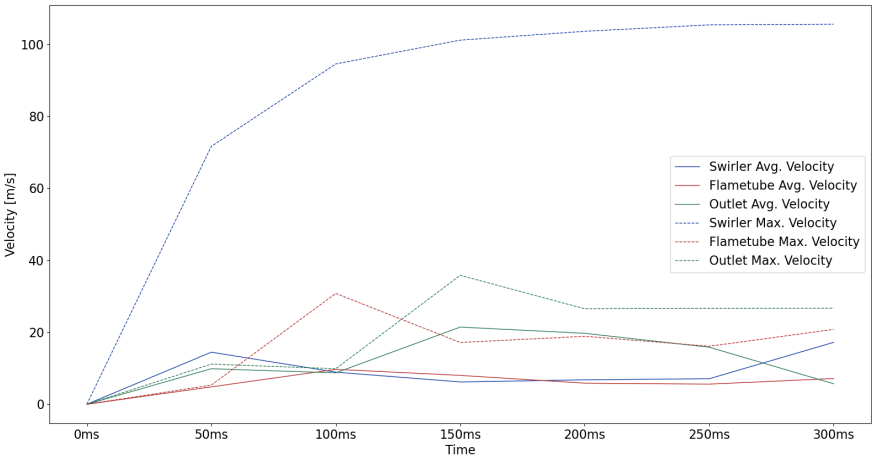

Figure 27: Average and Maximum Velocity over Time

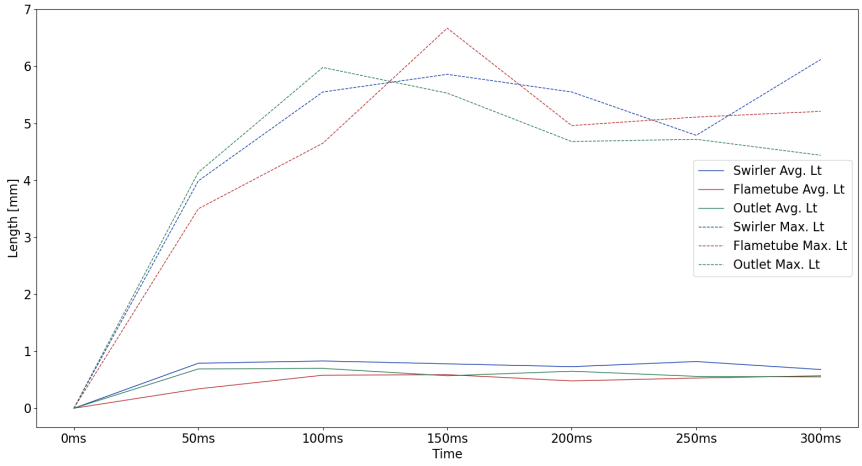

Figure 28: Average and Maximum Turbulent Length Scale over Time

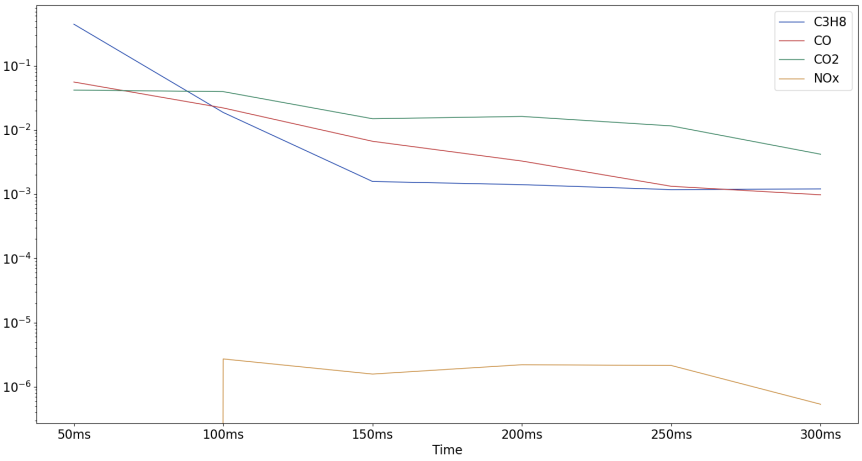

Figure 29: Average Mass Fractions of Species in Swirler over Time

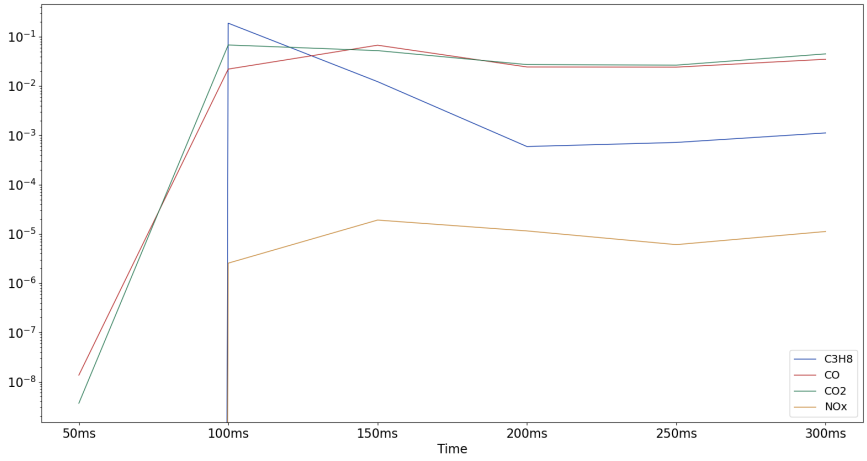

Figure 30: Average Mass Fractions of Species in Flametube over Time

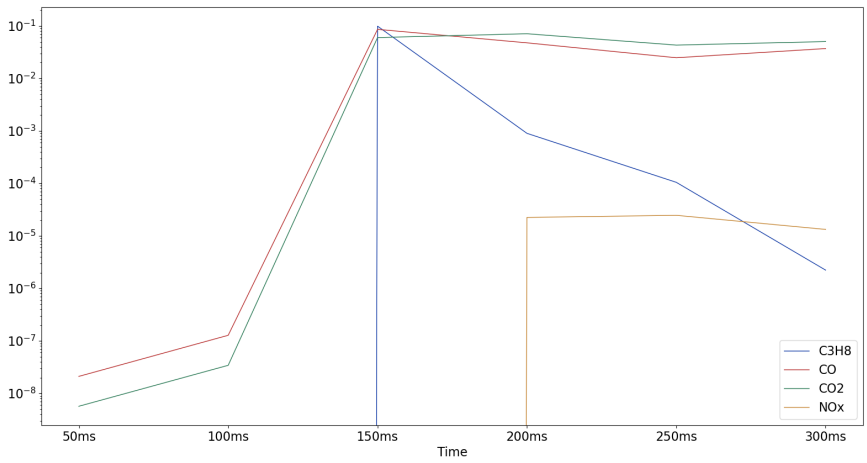

Figure 31: Average Mass Fractions of Species in Outlet over Time

5.2 Results of Experiment

5.2.1 Pressure Loss

Air flow was measured using a TMA10A anemometer with an accuracy of ±2%.

	Pressure [kPa]
At Inlet	4.06
At Outlet	2.03
Difference	2.03

Table 10: Pressure Loss

The pressure loss was relatively low compared to the fuel pressure (ranging between 6.8 to 20%). In most configurations the pressure loss should have a small impact on the results [34].

5.2.2 Temperature Distribution

The temperature sensors were RS PRO RS42 Digital Thermometers, with an error of ±0.5% [34].

	Test 1	**Test 2**	**Test 3**	**Test 4**
Fuel Pressure [bar]	1.0	3.0	2.0	1.8
Fuel Mass Flow [g/s]	0.81	-	1.32	1.38
Air Flow [l/s]	59.7	95.0	94.2	92.7
T_3 [K]	-	-	802	742
$T_{3,1}$ [K]	456	552	981	923
$T_{3,2}$ [K]	311	323	000	000
$T_{3,3}$ [K]	558	749	000	000

Table 11: Temperature Distribution.

5.2.3 Exhaust Gas

The chemical reaction which occurs when burning propane mainly involves hydrogen, carbon and oxygen. Carbon dioxide and water vapor is formed and heat is released. The chemical equation looks as follows:

$$C_3H_8 + 5O_2 \rightarrow 3CO_2 + 4H_2O$$

However, some undesired products are also formed in the process. Nitric oxide, more commonly known as NO_x molecules form when nitrogen in the air and water vapor from the combustion reacts at high temperature. The formation of NO_x can be retarded by reducing the combustion temperature. Combustion normally occurs at a temperature within the range of 1871-1927°C, at which the NO_x volume in the exhaust gas is around 0.01%. By lowering the temperature to below 1538°C the NO_x volume will be reduced to less than 20 ppm (0.002%).

$$2N + 5O + H_2O \rightarrow 2NO + 3O + H_2O \rightarrow 2HNO_3$$

Typically, low levels of NO_x gives high levels of carbon monoxide. If there is not sufficient oxygen present, incomplete combustion may occur and carbon monoxide forms:

$$2C_3H_8 + 9O_2 \rightarrow 4CO_2 + 2CO + 8H_2O$$

In addition sulfuric acid, another undesired product forms during combustion. The best way to reduce sulfuric acid is by removing as much sulfur as possible in the fuel.

$$H_2S + 4O \rightarrow SO_2 + H_2O \rightarrow H_2SO_4$$

The exhaust gas concentrations were measured using a Horiba PG 350E. It has a repeability of ±1%.

	Test 1	**Test 2**	**Test 3**	**Test 4**
Fuel Pressure [bar]	1	3	2	1.8
Fuel Mass Flow [g/s]	0.81	-	1.32	1.38
Air Flow [l/s]	59.7	95.0	94.2	92.7
NO_x [ppm]	7	9	0	0
CO [ppm]	424	1021	455	391
CO_2 [vol%]	2.69	4.49	1.9	1.82
O_2 [vol%]	16.77	13.9	18.04	18.18
SO_2 [ppm]	6.4	3.3	11.3	10.4

Table 12: Exhaust Gas Concentrations

NO_x levels were nearly zero when the fuel mass flow was increased. Increasing levels of CO_2 with increasing fuel pressure, while O_2 concentration decreases [34].

5.2.4 Measurement Errors

The combustor is not perfectly symmetrical, so the temperature sensors had a slightly different distance from the center of the liner. The Horiba PG 350E gas analyzer was calibrated for higher ppm levels, which may have affected its accuracy on low levels such as < 10 ppm.

6 Discussion

Temperature The temperature profile shows a good and well-centered temperature distribution throughout the combustor, which is beneficial for the material wear and lifetime. Large parts of the cross section have a relatively low temperature. In these parts, the combustion may be incomplete and lead to the formation of CO and unburned hydrocarbons. However, the temperature is exceeding 2200K in some areas in the center of the combustor, especially at the outlet. At this temperature, thermal NO_x will likely form. There are parts where the temperature exceeds 2200K, which indicates that NO_x will form during combustion. The combustor could benefit from measures to decrease the combustion temperature, especially at the outlet. In measuring points T3_1, T3_2 and T3_3, it was expected that there would be a deviation between the measured temperature and the converged values in the simulation. The temperature at these points will fluctate highly between time steps, as the rate of chemical reactions are still high in this portion of the combustor.

Velocity The flow velocity is quite uneven starting from the swirler and across the flametube. The air enters and is pushed to the top of the combustor, most likely due to the elbow shaped inlet pipe right before the swirler. To achieve a more even velocity profile, the combustor could probably benefit from having a straight air inlet pipe a longer portion behind the swirler.

Turbulent Length Scale The turbulence length scales develops quite early in the process and stays about the same throughout the whole process. Generally the flow is relatively laminar close to center where the fuel enters the combustor and in the air inlet. Turbulence is also low near the walls. It can clearly be seen that both the swirler and the flametube holes are generating turbulence in the flow, which improves mixing and enhances the reaction.

Emissions While CO_2 is naturally present in the combustor before the reaction even begins, CO actually forms relatively early in the process as well. The fuel does not reach the flametube and outlet part of the combustor before approximately 50-100ms into the process. As would be expected, NO_x is present where the temperature is high and doesn't start forming significantly before the 100ms mark. Conversely, CO tends to form in the areas rich with fuel and relatively low temperature. The concentration of CO

does however lower when getting closer to the outlet, as CO reacts with O_2 and forms CO_2. This might indicate that the actual CO emissions exiting the combustor is not necessarily very high.

The result of the simulation is of fair quality, but its accuracy could benefit from further mesh refinement and improved prism layer construction. Better hardware should have been used to generate a finer mesh and run the simulation with smaller time steps as well as more inner iterations per time step. Time steps for LES should preferrably be 1E-5s or smaller, as recommended in the STAR-CCM+ LES guidelines [35]. Using the coupled flow solver, instead of the segretated flow solver would also contribute to achieving an improved solution.

7 Conclusion

- An overview of the most common simulation methods for turbulent flow was presented.

- The LES turbulence model and fundamental equations used in CFD simulation tool STAR-CCM+ was described.

- Physics models, mesh generation and chemical reactions were set up in the software.

- After running the solvers for 220 hours, a result of fair quality was achieved. The main potential for improvement would be in better prism layer construction, mesh refinement and smaller time steps. Both the converged values and solution history results were presented.

- Reasons behind design choices of the combustor were explained.

- The combustor behaves as intended and the exhaust gas concentrations look fairly promising from an environmental friendly perspective, especially if a cooling technique would be implemented in an attempt to reduce the formation of NO_x. The read emission values are however subject to inaccuracy due to limitations of the measurement device and coarse simulation parameters.

- More time to solve and upgraded hardware would be beneficial for the accuracy of the simulation. This is especially the case when using the LES turbulence model, which is unsteady and require both fine time steps and a certain amount of iterations for each time step to converge sufficiently. The work done in this thesis could be replicated and improved upon by following the steps to set up the model in STAR-CCM+ and run with a finer mesh, smaller time steps and more iterations, resulting in a solution of higher quality.

References

[1] "Climate change, nasa," accessed February 06, 2020.

[2] C. N. Lane, *Acid rain: overview and abstracts*. Nova Publishers, 2003.

[3] R. Ehrlich and H. A. Geller, *Renewable energy: a first course*. CRC Press, 2017.

[4] R. L. Jaffe and W. Taylor, *The Physics of Energy*. Cambridge University Press, 2018.

[5] UCS, "Environmental impacts of natural gas, ucs," 2014, accessed February 06, 2020.

[6] H. I. Saravanamuttoo, G. F. C. Rogers, and H. Cohen, *Gas turbine theory*. Pearson Education, 2001.

[7] K. Brun and R. Kurz, *Compression Machinery for Oil and Gas*. Gulf Professional Publishing, 2018.

[8] T. Lieuwen, H. Torres, C. Johnson, and B. Zinn, "A mechanism of combustion instability in lean premixed gas turbine combustors," *J. Eng. Gas Turbines Power*, vol. 123, no. 1, pp. 182–189, 2001.

[9] R. Cant and E. Mastorakos, *An introduction to turbulent reacting flows*. Imperial College Press, 2008.

[10] B. L. Capehart, "Microturbines," 2016, accessed November 10, 2019.

[11] T. Giampaolo, *Gas turbine handbook: principles and practice*. Fairmont Press, 2002.

[12] MIT, "The brayton cycle, mit," 2006, accessed April 07, 2020.

[13] BP, "Natural gas, bp," 2019, accessed June 06, 2020.

[14] CIA, "The world factbook," 2017, accessed November 04, 2019.

[15] M. P. Boyce, *Gas turbine engineering handbook*. Elsevier, 2011.

[16] L. Møller-Pedersen, "Numerical study of a microturbine combustor," 2018.

[17] S. K, "Nox formation, k, sunil," 2002, accessed May 24, 2020.

[18] S. Amzin, "Computations of turbulent premixed flames using conditional moment closure," Ph.D. dissertation, University of Cambridge, 2012.

[19] A. Bakker, "Applied cfd - les," 2006, accessed May 23, 2020.

[20] Siemens, "Fundamental equations, the steve portal," accessed May 22, 2020.

[21] T. Poinsot and D. Veynante, *Theoretical and Numerical Combustion. 2nd Ed.* Edwards, 2005.

[22] Siemens, "Fluid flow, the steve portal," accessed May 23, 2020.

[23] ——, "Les, the steve portal," accessed April 08, 2020.

[24] ——, "Subgrid scale turbulence models, the steve portal," accessed May 23, 2020.

[25] ——, "Wall treatment, the steve portal," accessed May 23, 2020.

[26] ——, "Wall treatment for flow, the steve portal," accessed May 25, 2020.

[27] ——, "Wall treatment for les, the steve portal," accessed May 25, 2020.

[28] A. Bakker, "Solution methods," 2006, accessed May 17, 2020.

[29] Siemens, "Remedying cell quality, the steve portal," accessed May 31, 2020.

[30] Simwiki, "What is y+," accessed May 31, 2020.

[31] C. e. a. Kedar, "Boundary layer adaptivity for incompressible turbulent flow," *Scientific Computation Research Center*, p. 21, 2014.

[32] U. S. Diego, "The san diego mechanism, uc san diego," 2016, accessed May 27, 2020.

[33] A. Fontijn, A. J. Sabadell, and R. J. Ronco, "Homogeneous chemiluminescent measurement of nitric oxide with ozone. implications for continuous selective monitoring of gaseous air pollutants," *Analytical chemistry*, vol. 42, no. 6, pp. 575–579, 1970.

[34] H. Sørbotten and R. Fosse, "Nytt brennkammer til institutt for maskin- og marinfag sin modell-gassturbin," 2019.

[35] Siemens, "Les guidelines, the steve portal," accessed May 31, 2020.